J. Fluid Mech. (1990), *vol.* 215, *pp.* 23–44
Printed in Great Britain

The low-frequency scattering of Kelvin waves by stepped topography

By E. R. JOHNSON
Department of Mathematics, University College London, Gower Street, London WC1E 6BT, UK

(Received 1 March 1989)

A straightforward method that yields explicit transmission amplitudes is presented for Kelvin wave scattering by topography whose isobaths are parallel sufficiently far from the vertical, but not necessarily planar, wall supporting the incident wave. These results are obtained by first restricting attention to the low-frequency limit in which the flow splits naturally into three regions: an outer-x region containing the incident and transmitted Kelvin waves, an outer-y region containing outwardly propagating long topographic waves and an inner quasi-steady geostrophic region whose structure follows from earlier time-dependent analyses. The present analysis is further simplified by approximating general smooth features by stepped profiles with no restriction on the size, number or order of steps. Various qualitative results on the transmission amplitudes and flow fields are deduced from the explicit solutions and results are given on orthogonality, completeness and direction of propagation of the scattered long waves.

1. Introduction

In discussing tides in the English Channel, Lord Kelvin (Thomson 1879) introduced free-surface waves that propagate along bounding walls of a rotating fluid and decay exponentially away from the supporting wall. Subsequent analyses of these Kelvin waves by Taylor (1921), Miles (1972, 1973) and others have considered the effects of varying rotation rate, depth and boundary shape to provide models for seiches and tides in the North Sea and phase changes of tides passing over escarpments like that near Cape Mendocino. Such escarpments support subinertial topographic waves capable of carrying energy away from the coast. Miles (1973) explicitly excludes these effects from his analysis. It is the purpose of this and a companion paper (Johnson 1990*b*, referred to as II herein) to present results for Kelvin wave scattering by escarpments and more complex features extending far from the bounding wall and at frequencies sufficiently low that energy is removed from the scattering region by topographic waves. Progress is made possible by restricting attention to the low-frequency limit. Recent work on the related problem of the scattering of continental shelf waves (Johnson 1989*a*, *b*, *c*, *d*, 1990*a*) shows that many problems take particularly simple forms in this limit. Although the results are presented there under the rigid-lid assumption, it is noted that the analysis extends directly to free-surface flows and hence to the scattering of Kelvin waves. Some results for the special case of a single step have been presented by Johnson (1985), Gill *et al.* (1986) and Johnson & Davey (1990) who consider the temporal evolution of coastal currents above escarpments. Further results have been given by Killworth (1989*a*) who presents bounds for the amplitude of the transmitted Kelvin wave in the low-frequency limit

and numerical simulations for a particular ridge at various frequencies, remarking on the size and difficulty of the complex system of equations to be solved. The present analysis leads to a rapidly converging expression for the transmitted wave amplitude for arbitrary topography and to flow fields closely resembling those of the numerical simulations.

It is shown in §2 that in the low-frequency limit the flow separates naturally into three regions: an outer region varying slowly along the wall on the scale of the Kelvin wave, a second outer region varying slowly away from the wall on the scale of long topographic waves, and an inner, geostrophic region. The analysis of the present paper is further simplified by approximating arbitrary topography by stepped features, consisting of regions of constant height separated by vertical steps. This approximation is not restrictive. It enables very complicated profiles to be considered and gives equally accurate results far more economically when compared to explicit treatments of smooth ridges (see II). The discrete representation also appears more relevant to those used in ocean circulation models. In §3 results from previous time-dependent analyses of flow at upward and downward wall–step junctions are quoted to give the geostrophic region a set of linear constraints on the interface heights above the steps. These are combined with a radiation condition in §4 to give a reduced, real, linear system for the amplitude of the transmitted wave. The difficulties associated with the large complex system needed at arbitrary frequencies are avoided, as are the difficulties associated with smooth topography. Section 5 presents some results, general rules and flow patterns and §6 discusses briefly the extension to smooth topography, more general scattering regions, and stratified flow.

2. Equations of motion

The linear shallow-water equations can be written

$$\boldsymbol{u}_t + f\hat{\boldsymbol{z}} \wedge \boldsymbol{u} = -g\boldsymbol{\nabla} p, \tag{2.1}$$

$$\boldsymbol{\nabla} \cdot (H\boldsymbol{u}) = -p_t, \tag{2.2}$$

where $\boldsymbol{u}$ is the horizontal velocity, p the free surface displacement, H the local depth, f the Coriolis parameter, g gravitational acceleration and $\hat{\boldsymbol{z}}$ a unit vertical vector. Equation (2.1) can be rewritten as

$$(\partial_{tt} + f^2)\,\boldsymbol{u} = -g(\boldsymbol{\nabla} p_t - f\hat{\boldsymbol{z}} \wedge \boldsymbol{\nabla} p), \tag{2.3}$$

and so (2.2) gives the field equation

$$(\partial_{tt} + f^2)\,p_t - \boldsymbol{\nabla} \cdot [gH(\boldsymbol{\nabla} p_t - f\hat{\boldsymbol{z}} \wedge \boldsymbol{\nabla} p)] = 0. \tag{2.4}$$

On a solid boundary the normal component of $\boldsymbol{u}$ vanishes and so (2.3) gives

$$p_{nt} - fp_s = 0, \tag{2.5}$$

for outward normal n and arclength s.

Consider first the semi-infinite domain $-\infty < x^* < \infty$, $y^* \geqslant 0$ having an impermeable wall at $y^* = 0$ and topography depending on x^* alone, becoming flat for sufficiently large $|x^*|$, i.e. with

$$H = \begin{cases} H_0 & (x^* \to -\infty) \\ H_\infty & (x^* \to \infty), \end{cases} \tag{2.6}$$

for constants H_0, H_∞ (figure 1). More general domains and bottom topography are

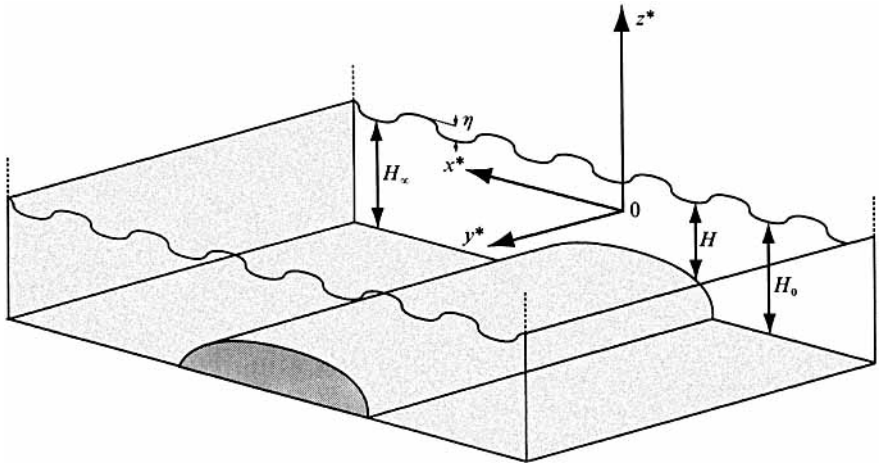

FIGURE 1. The simplest geometry considered. Topography depending on x^* alone abuts an impermeable wall at $y^* = 0$ bounding a semi-infinite ocean in $y^* \geqslant 0$, $-\infty \leqslant x^* \leqslant \infty$. More general geometries are considered in §6.

discussed in §6. Let a subinertial Kelvin wave of frequency ωf ($\omega < 1$) and unit amplitude be incident on the topography from $x^* = -\infty$, so

$$p \to \mathrm{e}^{-y} \cos[\omega(x - ft)] \quad (x \to -\infty), \tag{2.7}$$

where $(x, y) = (x^*, y^*)/a$ are scaled on the incident Rossby radius $a = (gH_0)^{\frac{1}{2}}/f$. Write $p = \mathrm{Re}\{\eta(x, y)\, \mathrm{e}^{\mathrm{i}\omega ft}\}$. Then η gives the scattered wave field provided

$$\mathrm{i}\omega[\nabla \cdot (h\nabla\eta) - (1-\omega^2)\,\eta] + \hat{\boldsymbol{z}} \cdot (\nabla h \wedge \nabla\eta) = 0 \quad (y > 0), \tag{2.8}$$

$$\mathrm{i}\omega\eta_y - \eta_x = 0 \quad (y = 0), \tag{2.9}$$

$$\eta \to \mathrm{e}^{-y - \mathrm{i}\omega x} \quad (x \to -\infty), \tag{2.10}$$

for $h(x) = H/H_0$. The incoming Kelvin wave is scattered by the ridge to give a transmitted Kelvin wave, evanescent Poincaré waves in the neighbourhood of the wall–ridge junction, and set of topographic waves, some evanescent and some propagating outwards along the ridge and decaying away from the ridge. Thus as $x \to \infty$

$$\eta \to A \exp\{-h_\infty^{-\frac{1}{2}}(y + \mathrm{i}\omega x)\}, \tag{2.11}$$

where $h_\infty = H_\infty/H_0$ and the complex amplitude A of the transmitted Kelvin wave is to be determined. Obtaining the amplitude and phase of the transmitted wave as a function of ridge height, width and profile at arbitrary frequencies can require a large numerical effort (Killworth 1989*a*) but straightforward solutions can be found in the low-frequency limit. The analysis is further simplified by considering ridges that are piecewise flat, i.e. with

$$h(x) = \begin{cases} 1 & (x < x_1) \\ h_j & (x_j < x < x_{j+1}) \\ h_n = h_\infty & (x_n < x), \end{cases} \tag{2.12}$$

having steps of height $h_j - h_{j-1}$ at the n points $x_1, \ldots, x_n$. With this topography, field equation (2.8) becomes

$$h_j \nabla^2\eta - (1-\omega^2)\,\eta = 0 \quad (x_j < x < x_{j+1}, j = 0, \ldots, n), \tag{2.13}$$

with the jump conditions

$$[\eta] = 0, \quad i\omega[h\eta_x] + [h]\eta_y = 0 \quad (x = x_j, \quad j = 1, \ldots, n), \tag{2.14}$$

introducing for compactness the convention $x_0 = -\infty, x_{n+1} = \infty$. There are three distinct regions in the limit $\omega \to 0$. Denote as the inner region the region with x, y fixed as $\omega \to 0$, as the outer-x region the region with $X = \omega x$, y fixed, and as the outer-y region the region with $x, Y = \omega y$ fixed. The fourth possibility of X, Y fixed gives the quiescent ocean $\eta \equiv 0$.

The outer-x region is trivial. Here (2.13), (2.19) become

$$\eta_{yy} - \eta = 0 \quad (X < 0), \quad h_\infty \eta_{yy} - \eta = 0 \quad (X > 0), \tag{2.15}$$

$$i\eta_y - \eta_X = 0 \quad (y = 0, \quad X \neq 0), \tag{2.16}$$

with solution given by the Kelvin waves of (2.10), (2.11), i.e.

$$\eta = \begin{cases} \exp[-(y + iX)] & (X < 0) \\ A \exp[-h_\infty^{-\frac{1}{2}}(y + iX)] & (X > 0), \end{cases} \tag{2.17}$$

and the ridge appearing as a singularity along $X = 0$.

3. The inner region

In the present low-frequency limit, (2.3) shows that the inner region is geostrophic and no flow crosses any step in $y > 0$, i.e. since η_y vanishes on $x = x_i$ by (2.14),

$$\eta = \eta_j \quad (x = x_j, \quad j = 1, \ldots, n), \tag{3.1}$$

for (unknown) constants η_j. Similarly η_x vanishes on $y = 0$ by (2.9) so

$$\eta = a_j \quad (x_j < x < x_{j+1}, y = 0, \quad j = 1, \ldots, n) \tag{3.2}$$

for (unknown) amplitudes a_j. Since the limit $X \to 0$ of (2.17) matches (3.2),

$$a_0 = 1, \quad a_n = A. \tag{3.3}$$

Consider the wall–step junction at x_j. Sufficiently close to the junction, equations (2.13), (2.14), (2.15) reduce to the rigid-lid flow over a single step, solved for arbitrary frequencies in Johnson (1985). For an upward step $h_j < h_{j-1}$ all waves propagate outwards, information travels away from the wall and the junction is non-singular with surface elevation continuous across x_j. Thus

$$a_{j-1} = \eta_j = a_j \quad \text{for} \quad h_j < h_{j-1}. \tag{3.4}$$

Energy is conserved at the junction. For a downward step waves generated in the start-up of the periodic forcing (2.10) carry information towards the wall. The continuous arrival of energy forces a singularity there with the entire incident mass flux passing through the singularity. Since η is a stream function for the motion in this region, conservation of mass gives

$$h_{j-1}(a_{j-1} - \eta_j) = h_j(a_j - \eta_j) \quad \text{for} \quad h_j > h_{j-1},$$

i.e.

$$\eta_j = (h_j a_j - h_{j-1} a_{j-1})/(h_j - h_{j-1}) \quad \text{for} \quad h_j > h_{j-1}. \tag{3.5}$$

For a single step ($\eta_j = 0$, see §5), (3.5) reduces to the result in Gill *et al.* (1986) verified by the numerical integrations of Johnson & Davey (1990). The free surface is discontinuous across the singularity ($a_j \neq a_{j-1}$) and energy is not conserved, with

more energy carried inwards by the incident Kelvin and topographic waves than transported away by the sole transmitted Kelvin wave. This is a consequence of the absence of short waves above vertical steps. Above steep, but not vertical, downward steps short waves are present with phase propagating towards the wall but carrying energy slowly outwards from the wall. For vertical steps the energy that would otherwise be carried outwards by short waves remains trapped at the wall. In the low-frequency limit, approximating continuous topography by a stepped obstacle corresponds to the weakly dissipative flows of Johnson (1989*a*, *b*) where even vanishingly small viscosity destroys short wave energy in a boundary layer of thickness ω against the wall. Short waves carrying energy outwards are present above downward slopes for completely inviscid flow over continuous topography and energy is conserved even in the low-frequency limit (Johnson 1990*a*). The long-wave field is, however, unaltered from the weakly dissipative determination and so although not determining the short-wave field for inviscid flow, the present approximation gives the inviscid long-wave field. The dissipative layer and short-wave fields are discussed in detail in II.

Denote by $I(j)$ the cumulative number of downward steps for $x \leqslant x_j$, up to and including the step at x_j, with $I(0) = 0$. Then there are $I(n) = m$ (say) downward steps and $n-m$ upward steps altogether. At an upward step no new unknowns enter the problem, η_j and a_j being determined by a_{j-1}. At a downward step one new unknown enters. Take this to be a_j, the free surface height along the wall after the step. The free surface retains this constant height until the next downward step. Denote these (unknown) heights by $b_1, \ldots, b_m$ (with $b_0 = a_0$). Then the interface heights along the wall are given by

$$\eta = a_j = b_{I(j)} \quad (x_j \leqslant x < x_{j+1}, \quad j = 0, \ldots, n) \tag{3.6}$$

and the interface height along the step $x = x_j$ by

$$\eta = \eta_j = \begin{cases} b_{I(j-1)} & \text{if } h_j < h_{j-1} \\ [h_j b_{I(j)} - h_{j-1} b_{I(j-1)}]/(h_j - h_{j-1}) & \text{if } h_j > h_{j-1}. \end{cases} \tag{3.7}$$

Introducing the $n \times 1$ and $(m+1) \times 1$ vectors $\boldsymbol{\eta} = (\eta_1, \ldots, \eta_n)^{\mathrm{T}}$ and $\boldsymbol{b} = (b_0, b_1, \ldots, b_m)^{\mathrm{T}}$ allows (3.7) to be written

$$\boldsymbol{\eta} = \boldsymbol{B}\boldsymbol{b} \tag{3.8}$$

where $\boldsymbol{B}$ is lower tridiagonal $n \times (m+1)$, and the m rows corresponding to the m downward steps are linearly independent. The determination of $\boldsymbol{b}$ is discussed in §4.

Once $\boldsymbol{b}$ and so the a_j and η_j are known, the value of η for all x, y follows straightforwardly. For $x_j < x < x_{j+1}$, (2.13) becomes

$$h_j \nabla^2 \eta - \eta = 0, \tag{3.9}$$

subject to

$$\eta = \eta_j \quad (x = x_j), \quad \eta = \eta_{j+1} \quad (x = x_{j+1}), \tag{3.10}$$

$$\eta = a_j \quad (y = 0) \quad \nabla\eta \quad \text{bounded} \quad (|x|, y \to \infty). \tag{3.11}$$

The solution of (3.9), (3.10), (3.11) can be written

$$\eta = a_j \exp(-h_j^{-\frac{1}{2}} y) + \frac{2}{\pi} \int_0^\infty P(x, l) \sin ly \, \mathrm{d}l \quad (x_j \leqslant x \leqslant x_{j+1}), \tag{3.12}$$

where

$$P(x,l)=\begin{cases}(\eta_1/l-la_0/\kappa_0^2)\exp[\kappa_0(x-x_1)] & (x\leqslant x_1)\\ \{(\eta_j/l-la_j/\kappa_j^2)\sinh[\kappa_j(x_{j+1}-x)]+(\eta_{j+1}/l-la_j/\kappa_j^2)\\ \qquad\times\sinh[\kappa_j(x-x_j)]\}/\sinh[\kappa_j(x_{j+1}-x_j)] & (x_j\leqslant x\leqslant x_{j+1})\\ (\eta_n/l-la_n/\kappa_n^2)\exp[-\kappa_n(x-x_n)] & (x\geqslant x_n),\end{cases} \tag{3.13}$$

where $\kappa_j=(l^2+h_j^{-1})^{\frac{1}{2}}$. The surface elevation becomes independent of y exponentially fast with distance from the wall,

$$\eta\to F(\boldsymbol{\eta};x)=\begin{cases}\eta_1\exp(x-x_1) & (x\leqslant x_1)\\ \{\eta_j\sinh[h_j^{-\frac{1}{2}}(x_{j+1}-x)]+\eta_{j+1}\sinh[h_j^{-\frac{1}{2}}(x-x_j)]\}/\sinh\Delta_j\\ \qquad\times(x_j\leqslant x\leqslant x_{j+1},\quad j=1,\ldots,n-1)\\ \eta_n\exp[-h_n^{-\frac{1}{2}}(x-x_n)] & (x\geqslant x_n),\end{cases} \tag{3.14}$$

where $\Delta_j=h_j^{-\frac{1}{2}}(x_{j+1}-x_j)$. The value of F at a given x depends solely on the components of $\boldsymbol{\eta}$, i.e. on the interface heights above the steps. Expression (3.14) provides the inner boundary condition for the outer-y solution of the following section.

4. The outer-y region

Here (2.13), (2.14) become

$$h_j\eta_{xx}-\eta=0\quad(x_j<x<x_{j+1},\quad j=0,\ldots,n), \tag{4.1}$$

$$[\eta]=0,\quad \mathrm{i}[h\eta_x]+[h]\eta_Y=0\quad(x=x_j,\quad j=1,\ldots,n) \tag{4.2}$$

with

$$\eta\to 0\quad(|x|\to\infty), \tag{4.3}$$

to match the quiescent outer ocean. System (4.1)–(4.3) describes long topographic waves propagating along the feature. The waves are non-dispersive with energy and phase travelling in the same direction. From (4.2) the system has wave-like solutions of the form

$$\eta=\mathrm{e}^{\mathrm{i}lY}F_l(x) \tag{4.4}$$

provided

$$h_jF_l''-F_l=0\quad(x_j<x<x_{j+1},\quad j=0,\ldots,n), \tag{4.5}$$

$$[F_l]=0\quad(x=x_j,\quad j=1,\ldots,n), \tag{4.6}$$

$$[hF_l']+l[h]F_l=0\quad(x=x_j,\quad j=1,\ldots,n) \tag{4.7}$$

$$F_l\to 0\ (|x|\to\infty). \tag{4.8}$$

The solution of (4.5), (4.6) and (4.8) is determined by the values of F at the steps x_j. Comparison with (3.14) gives the general solution

$$F_l(x)=F(\boldsymbol{f};x), \tag{4.9}$$

where $F(\boldsymbol{f};x_j)=f_j$ and the vector $\boldsymbol{f}=(f_1,\ldots,f_n)^{\mathrm{T}}$ gives the surface elevations above the step. Substituting (4.9) in the jump condition (4.7) gives the recurrence relation

$$l(h_j-h_{j-1})f_j=-h_{j-1}^{\frac{1}{2}}\operatorname{cosech}\Delta_jf_{j-1}+(h_{j-1}^{\frac{1}{2}}\coth\Delta_j+h_j^{\frac{1}{2}}\coth\Delta_{j+1})f_j-h_j^{\frac{1}{2}}\operatorname{cosech}\Delta_{j+1}f_{j+1}, \tag{4.10}$$

and thus the algebraic eigenvalue problem

$$\boldsymbol{A}\boldsymbol{f}=l\boldsymbol{D}\boldsymbol{f}, \tag{4.11}$$

where $\boldsymbol{A}$ is real, symmetric, tridiagonal and (since $\coth \Delta_j > \operatorname{cosech} \Delta_j$) diagonally dominant and $\boldsymbol{D}$ is real and diagonal with elements

$$D_{jj} = h_j - h_{j-1}, \tag{4.12}$$

positive for the m downward steps and negative for the $n-m$ upward steps.

Since $\boldsymbol{A}$ is diagonally dominant a straightforward application of Gershgorin's theorem (Golub & Van Loan 1983) shows that each eigenvalue of $\boldsymbol{A}$ has positive real part. Since $\boldsymbol{A}$ is real, symmetric all eigenvalues of $\boldsymbol{A}$ are real. Thus all eigenvalues of $\boldsymbol{A}$ are real and positive. Hence $\boldsymbol{A}$ is positive definite.

Since $\boldsymbol{A}$ is symmetric positive definite and $\boldsymbol{D}$ is symmetric the eigenvalues of the generalized eigenvalue problem (4.11) are real. Moreover applying Gershgorin's theorem to the diagonally dominant but not symmetric $\boldsymbol{D}^{-1}\boldsymbol{A}$ shows that there are as many eigenvalues with positive real parts as there are positive D_{jj} and as many with negative real parts as there are negative D_{jj}. Thus the eigenvalues of (4.11) can be written

$$\lambda_1 \geqslant \lambda_2 \geqslant \ldots \geqslant \lambda_m > 0 > \lambda_{m+1} \geqslant \ldots \geqslant \lambda_n. \tag{4.13}$$

From (4.4) positive eigenvalues correspond to waves propagating towards the wall and thus, as in §3, there exist m inwardly propagating waves corresponding to the m downward steps and $n-m$ outwardly propagating waves corresponding to the $n-m$ upward steps.

Since $\boldsymbol{A}$ is symmetric positive definite it furnishes the inner product and norm

$$\langle \boldsymbol{f}_1, \boldsymbol{f}_2 \rangle = \boldsymbol{f}_1^{\mathrm{T}} \boldsymbol{A} \boldsymbol{f}_2, \quad \|\boldsymbol{f}\|^2 = \langle \boldsymbol{f}, \boldsymbol{f} \rangle. \tag{4.14}$$

Since $\boldsymbol{D}$ is symmetric it follows that to each λ_j there corresponds one real eigenvector $\boldsymbol{\xi}_j$ (say) and that the eigenvectors corresponding to distinct eigenvalues are orthogonal (and any corresponding to repeated eigenvalues can be so constructed). Thus any vector $\boldsymbol{f}$ can be written as

$$\boldsymbol{f} = \sum_{j=1}^{n} \alpha_j \boldsymbol{\xi}_j \quad \text{with} \quad \alpha_j = \langle \boldsymbol{f}, \boldsymbol{\xi}_j \rangle / \|\boldsymbol{\xi}_j\|^2. \tag{4.15}$$

Note that $\boldsymbol{f}_1^{\mathrm{T}} \boldsymbol{D} \boldsymbol{f}_2$ does not yield a positive definite inner product for topography containing both upward and downward steps since by (4.11) and (4.13)

$$\boldsymbol{\xi}_j^{\mathrm{T}} \boldsymbol{D} \boldsymbol{\xi}_j = \lambda_j^{-1} \boldsymbol{\xi}_j^{\mathrm{T}} \boldsymbol{A} \boldsymbol{\xi}_j \begin{cases} > 0 & \text{if } j = 1, \ldots, m \\ < 0 & \text{if } j = m+1, \ldots, n, \end{cases} \tag{4.16}$$

i.e. there would exist vectors with negative norms and non-zero vectors with zero norm. For computational purposes it is convenient however to note from (4.11) the alternative expression for the α_j in (4.15),

$$\alpha_j = \boldsymbol{f}^{\mathrm{T}} \boldsymbol{D} \boldsymbol{\xi}_j / \boldsymbol{\xi}_j^{\mathrm{T}} \boldsymbol{D} \boldsymbol{\xi}_j \quad (j = 1, \ldots, n), \tag{4.17}$$

where the denominator is non-zero since $\|\boldsymbol{\xi}_j\| > 0$ and by (4.13). The inner product (4.14) is the low-frequency, free-surface, discrete form of the inner product introduced in Johnson (1989*d*). The continuous form is given in II. They differ from the usual inner product and norm (Huthnance 1975; Killworth 1989*a*), which correspond to the quadratic form $\boldsymbol{f}_1^{\mathrm{T}} \boldsymbol{D} \boldsymbol{f}_2$, in remaining positive definite for topography with slopes of both signs.

The general solution of (4.1)–(4.3) satisfying the radiation condition that no energy travels inwards from $Y = \infty$ can thus be written

$$\eta(x, Y) = \sum_{j=m+1}^{n} \beta_j F(\boldsymbol{\xi}_j; x) \, \mathrm{e}^{\mathrm{i}\lambda_j Y}, \tag{4.18}$$

where the $n-m$ coefficients $\beta_{m+1}, \ldots, \beta_n$ and the m amplitudes $b_1, \ldots, b_m$ are determined by matching (4.18) at $Y = 0$ with (3.14), and can be taken as real since the ξ_j, λ_j are. The surface elevation is thus given in the outer-y region by

$$p(x, Y, t) = \sum_{j=m+1}^{n} \beta_j F(\xi_j; x) \cos(\lambda_j Y + \omega f t), \tag{4.19}$$

with each mode propagating outwards with dimensional speed

$$\frac{dy^*}{dt} = (gH_0)^{\frac{1}{2}}/(-\lambda_j). \tag{4.20}$$

Since the cross-ridge profiles of (4.18) at $Y = 0$ and (3.14) are of the same form it is sufficient to match at the steps alone. This gives n equations

$$\sum_{j=m+1}^{n} \beta_j \xi_j = \boldsymbol{\eta} = \boldsymbol{B}\boldsymbol{b}, \tag{4.21}$$

relating the $n+1$ unknowns $b_0, b_1, b_2, \ldots, b_m, \beta_{m+1}, \ldots, \beta_n$. The unknown β_j can be eliminated by multiplying both sides of (4.21) by the $m \times n$ matrix $\boldsymbol{ED}$ where $\boldsymbol{E}^{\mathrm{T}}$ is the $n \times m$ matrix of eigenvectors corresponding to incoming waves, i.e.

$$\boldsymbol{E}^{\mathrm{T}} = (\xi_1, \xi_2, \ldots, \xi_m). \tag{4.22}$$

Then by orthogonality

$$\boldsymbol{EDB}\boldsymbol{b} = 0. \tag{4.23}$$

Equation (4.23) determines $\boldsymbol{b}$ as the sole vector in the null space of the rank m matrix $m \times (m+1)$ matrix $\boldsymbol{EDB}$. The ratio b_m/b_0 is real and gives the amplitude of the transmitted Kelvin wave for an incident wave of unit amplitude. There is no change in phase in the outer-x region of the wave in crossing the ridge nor any phase change in the other regions, irrespective of the shape or height of the ridge.

The $n \times (m+1)$ matrix $\boldsymbol{DB}$ is particularly simple with zero entries except for

$$\left.\begin{aligned} &(\boldsymbol{DB})_{jk} = h_j - h_{j-1} \quad (I(k-1) < j < I(k)), \\ &(\boldsymbol{DB})_{jk} = -h_{j-1} \quad (\boldsymbol{DB})_{jk+1} = h_j \quad (j = I(k)). \end{aligned}\right\} \tag{4.24}$$

Once $\boldsymbol{b}$ has been determined from (4.23), the coefficients β_j of the outward propagating waves are given explicitly from (4.17) by

$$\beta_j = \boldsymbol{\xi}_j^{\mathrm{T}} \boldsymbol{DBb} / \boldsymbol{\xi}_j^{\mathrm{T}} \boldsymbol{D}\boldsymbol{\xi}_j, \tag{4.25}$$

and the vector $\boldsymbol{\eta}$ follows from (3.8). The solution is complete.

5. Examples

If the ridge is a downward escarpment, consisting of only downward steps, then all the incident volume flux is constrained to pass through each wall–step singularity and finally emerge at the far side of the escarpment. Conservation of mass then gives

$$\left.\begin{aligned} &\eta_j = 0, \\ &a_j = (h_{j-1}/h_j)\, a_{j-1} \end{aligned}\right\} \quad (j = 1, \ldots, n), \tag{5.1}$$

and so the amplitude of the transmitted wave is reduced by a factor $H_0/H_\infty < 1$. If the ridge is an upward escarpment, consisting of only upward steps, then the

wall–step junctions are non-singular and free-surface elevation is continuous along the wall, i.e.

$$\left.\begin{aligned}\eta_j &= 1\\ a_j &= 1\end{aligned}\right\} \quad (j = 1, \ldots, n), \tag{5.2}$$

and the amplitudes of the incident and transmitted waves are equal. These are precisely the results given in Gill *et al.* (1986), and extend directly to continuous escarpments to give the same transmission amplitudes but, for downward escarpments, with a dissipative boundary layer or short waves carrying energy outwards and continuous variation of η along the wall (see II).

If the topography consists of upward and downward escarpments separated from each other by more than three or so Rossby radii their interactions are negligible and (5.1) and (5.2) can be applied consecutively. In particular, a ridge with a wide flat top separating ocean of constant depth (i.e. $h_\infty = h_0$), transmits a Kelvin wave with amplitude diminished by the factor $H_1/H_0 < 1$ where H_1 is the depth over the ridge. A wide flat valley in the same ocean transmits a Kelvin wave with amplitude diminished by the factor $H_0/H_1 < 1$ where H_1 is again the depth over the feature. Wide features with reciprocal extrema of fractional depth have the same amplitude of transmitted wave.

A second type of simple explicit solution is given by a ridge consisting of two steps ($n = 2$) of opposite sign ($m = 1$). Choose the origin such that $x_{1,2} = \pm W$ and let $H_\infty = H_0$ so the depth after the ridge equals the depth before. Then the amplitude of the transmitted wave depends solely on the ridge half-width W and the fractional depth over the ridge, $h_1 = H_1/H_0$. The eigenvalue problem (4.11) gives the real equal and opposite (since the topography is symmetric) wavenumbers

$$\lambda_{1,2} = \pm(1 + 2h_1^{\frac{1}{2}} \coth W_1 + h_1)^{\frac{1}{2}}/(1 - h_1), \tag{5.3}$$

where $W_1 = 2W/h_1^{\frac{1}{2}}$. For a ridge ($h_1 < 1$) the outward propagating wave ($\lambda_2 < 0$) is given by the negative sign in (5.3). The corresponding eigenvector can be written $\boldsymbol{\eta} = (1, \gamma)^{\mathrm{T}}$ where

$$\gamma = h_1^{-\frac{1}{2}} \sinh W_1 [1 + h_1^{\frac{1}{2}} \coth W_1 - (1 + 2h_1^{\frac{1}{2}} \coth W_1 + h_1)^{\frac{1}{2}}]. \tag{5.4}$$

The junction at x_1 is non-singular so $\eta_1 = 1$, the incident amplitude, and the junction at x_2 is singular with conservation of mass giving the amplitude of the transmitted Kelvin waves as

$$A = h_1 + (1 - h_1)\eta_2 = h_1 + (1 - h_1)\gamma. \tag{5.5}$$

For a valley ($h_1 > 1$) the outward propagating wave is given by the positive sign in (5.3). The corresponding eigenvector can be written $(\gamma, 1)^{\mathrm{T}}$. The junction at x_2 is non-singular so $\eta_2 = A$, the transmitted amplitude, and the junction at x_1 is singular with conservation of mass giving

$$A = h_1^{-1} + (1 - h_1^{-1})\eta_1 = h_1^{-1} + (1 - h_1^{-1})\gamma A$$

so

$$A = [h_1 + (1 - h_1)\gamma]^{-1}. \tag{5.6}$$

For currents whose width above the feature is small compared to the width of the feature ($h_1^{\frac{1}{2}} \ll W$), (5.4) gives $\gamma = 0$ and (5.5) and (5.6) reduce to the asymptotic forms for wide ridges given above. For narrow features ($W \ll h_1^{\frac{1}{2}}$), $\gamma = 1$ and transmission is perfect. Figure 2(*a*) gives the amplitude A as a function of ridge half-width for various feature depths. The amplitudes rapidly attain their asymptotic value with increasing W, being within 10% by $W = 0.5$ for all but the deepest of valleys. The behaviour of ridges and their corresponding reciprocal valleys is closest for small

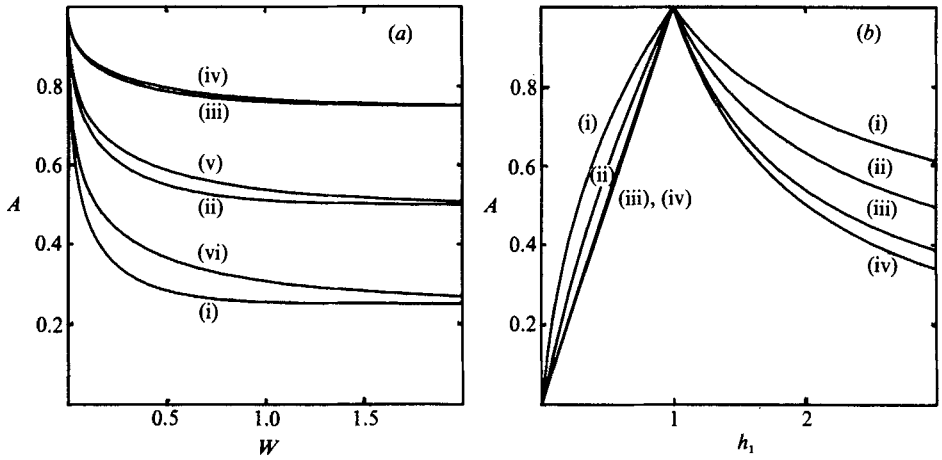

FIGURE 2. (*a*) The amplitude A of the transmitted Kelvin wave for an incident wave of unit amplitude for a rectangular ridge as a function of the ridge half-width W. The depths above the feature, scaled on the far-field depth are (i) $h_1 = \frac{1}{4}$, (ii) $\frac{1}{2}$, (iii) $\frac{3}{4}$, (iv) $\frac{4}{3}$, (v) 2, (vi) 4. For narrow features transmission is perfect. For wide features transmission for ridges of minimum depth h_1 is the same as that for valleys of maximum depth $1/h_1$. (*b*) The transmitted amplitude as a function of h_1 for half-widths (i) $W = 0.1$, (ii) 0.3, (iii) 1, (iv) 3. By $W = 3$, A varies linearly with h_1 for ridges ($h_1 < 1$) and inversely as h_1 for valleys ($h_1 > 1$).

features, diverging as the heights of the features, and so the disparities in Rossby radii above the features, increase. Figure 2(*b*) gives A as a function of h_1 for increasing widths. For ridges ($H_1 < H_0$) the transmitted amplitude is indistinguishable from the asymptotic ($W \ll 1$) linear variation by $W = 1$. The deviation from wide-feature asymptotics is significantly larger for valleys ($H_1 > H_0$) owing to their larger above-feature Rossby radius.

The bounds on the transmission amplitude in Killworth (1989*a*) can be written $\sigma \leqslant A \leqslant \sigma^{\frac{1}{2}}$ where

$$\sigma = [h_1 + (2 - h_1)\gamma]/[2 - h_1 + h_1\gamma]. \tag{5.7}$$

Figure 3(*a*) shows the variation in the bounds and the exact value as a function of W for various h_1. The bounds are most accurate for low narrow features, becoming less accurate for larger features. The hypothesis of Killworth (1989*a*, *b*) that the upper bound is always attained is not borne out. It is shown in II that this follows from the neglect of the order-one energy carried outwards by short waves in inviscid flow (Johnson 1990*a* and visible in the numerical simulations of Killworth 1989*a*) or destroyed at the wall in weakly dissipative flow (Johnson 1989*a*) and above stepped features. Only when the topography is an upward escarpment, so no short waves are present and the transmitted amplitude is unity, is the bound achieved. For a valley the bounds give $\sigma^{-1} \leqslant A \leqslant \sigma^{-\frac{1}{2}}$. Figure 3(*b*) shows the bounds and the exact solution. For $h_1 > 2$ the lower bound vanishes and the upper bound becomes undefined at some finite W. This again follows from the neglect of short waves and occurs for any feature containing a sufficiently wide, deep valley. Examples for continuous topography are given in II together with an accurate one-mode estimate for the transmitted amplitude. The estimate coincides with the exact values (5.5) and (5.6) in the present case as no other modes are present.

Figures 4 and 5 give the flow patterns in the inner and outer regions for a wide high ridge ($W = 2, h_1 = H_1/H_0 = 1/2$) and a wide, deep valley ($W = 2, h_1 = 2$). In both

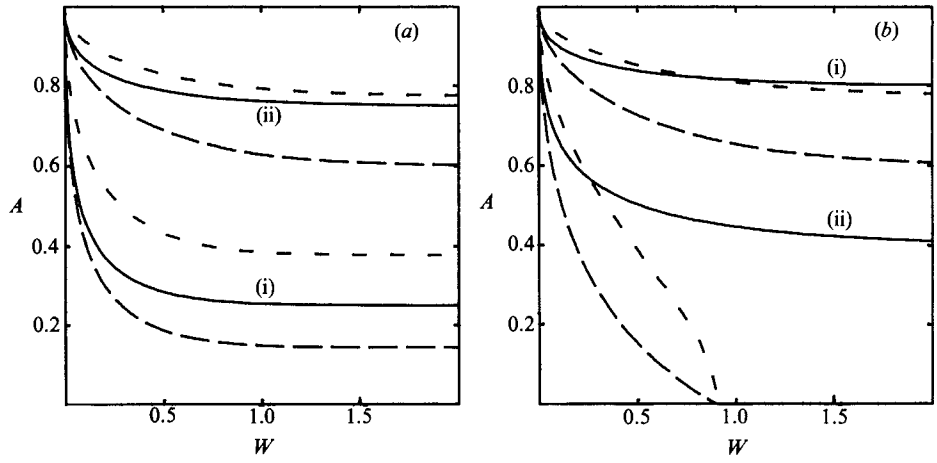

FIGURE 3. The amplitude of the transmitted Kelvin wave (solid line) with the upper (short dash) and lower (long dash) bounds from Killworth (1989*a*) for a rectangular feature as a function of the half-width W. (*a*) A ridge with (i) $h_1 = \frac{1}{4}$ and (ii) $\frac{3}{4}$. (*b*) A valley with (i) $h_1 = \frac{5}{4}$ and (ii) $\frac{5}{2}$.

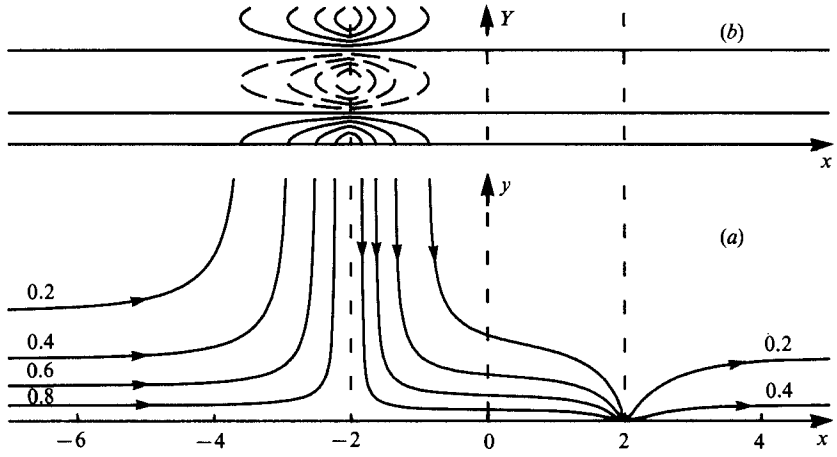

FIGURE 4. Contours of free-surface elevation p for a ridge of half-width $W = 2$ and minimum depth $h_1 = \frac{1}{2}$. In this and the succeeding patterns of p the three vertical dashed lines give the start, middle and end of the topography. (*a*) On the inner scale the contours are streamlines. The arrows and amplitudes correspond to the time of maximum positive amplitude of the incident Kelvin wave. (*b*) On the outer-y scale, with $Y = \omega y$. The contours interval is the same as in (*a*) with negative values shown broken. The pattern is shown at the same instant as (*a*) joining continuously at $Y = 0$ to the solution as $y \to \infty$ and turning the outward flux in $x < -W$ to return above the ridge in $x > W$.

cases the transmitted amplitude is 0.25 as expected. In the inner region, parts (*a*) of the figures, since η is real,

$$p(x, y, t) = \eta(x, y) \cos \omega f t, \tag{5.8}$$

and so, from (2.3), η gives the streamlines of flow. During one period the signed magnitude of the velocity at any point varies sinusoidally but its direction is fixed. The arrows give the direction of flow for that half of the period for which the Kelvin elevation is positive and are reversed for the other half. For the ridge the incident flux is turned to flow outwards beside the ridge returning as a current of the same amplitude above the ridge. Since the depth over the ridge is $\frac{1}{2}H_0$ the flux associated

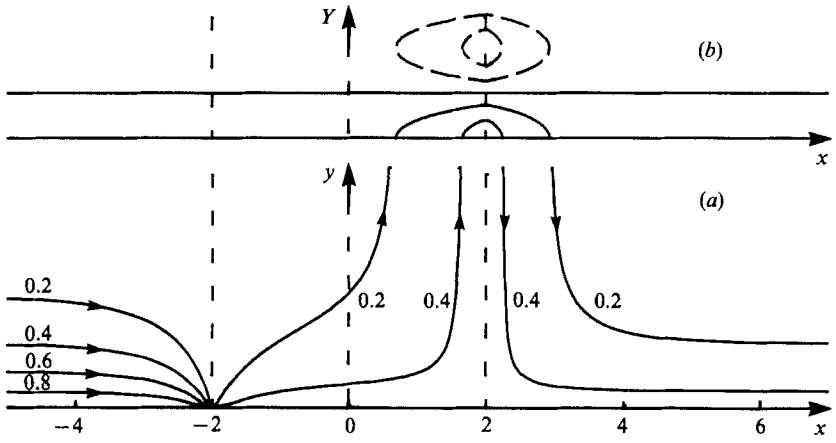

FIGURE 5. As for figure 4 but for a valley of depth $h_1 = 2$. The radiated wave field is weaker and the current over the feature less confined although the transmitted amplitude is unaltered.

with current is decreased to 0.5. The return flow is turned to continue as a Kelvin wave along the wall, passing through a singularity at $(2, 0)$ where the volume flux is conserved but the wave amplitude decreases owing to the increase in depth. For the valley the volume flux is conserved in passing through the singularity at $(-2, 0)$ but the amplitude decreases to 0.5 as the depth increases. The larger Rossby radius above the valley means that the outward flow is less confined and reflects the slower approach above the deep valleys to the asymptotic form for wide features ($W \gg 1$). The flow on the far side of the valley has the same amplitude as the outward flow and thus returns only half its flux. Parts (*b*) of the figures show contours of the free-surface elevation in the outer region as given by (4.19). Since only one wave is present the patterns propagate outwards without change of form joining continuously at $Y = 0$ to the limit $y \to \infty$ of the inner solutions. In both cases the wave is concentrated over the upward step, having amplitude above the ridge determined by the incident wave and thus larger than that above the valley, determined by the transmitted wave. Figures 6 and 7 give the same flow patterns for narrower features, of half-width $W = 0.3$. Although the individual Kelvin wave components can be clearly identified away from the features, above them the flow is strongly confined by the steps, remaining parallel until close to the wall. The outer flow patterns show that the waves, concentrated over the upward step, no longer have negligible amplitude by the downward step. The return current above the ridge thus extends slightly into $x > W$ and some fluid (with $p \leqslant 0.2$) turns to join the transmitted wave without passing through the singularity at $(W, 0)$. This bypassing of the singularity shows more clearly in the outer flow over the valley since the current is even less confined owing to the larger Rossby radius associated with the valley. For the same reason the transmitted wave is even larger for the valley than for the ridge although both transmit more than their wider counterparts.

Explicit solutions can be obtained for features containing up to four steps (requiring the roots of a quartic) but lack the simplicity of the general formulation. For more complex features, and approximation to smooth features, consider the stepped topography obtained by dividing the interval where $h(x)$ differs from its far-field values into $n-1$ strips of constant depth given by the value of h at the midpoint of the strip. This choice preserves the cross-sectional area of piecewise linear features. In the examples to follow the strips are chosen to be of equal width. This choice leads

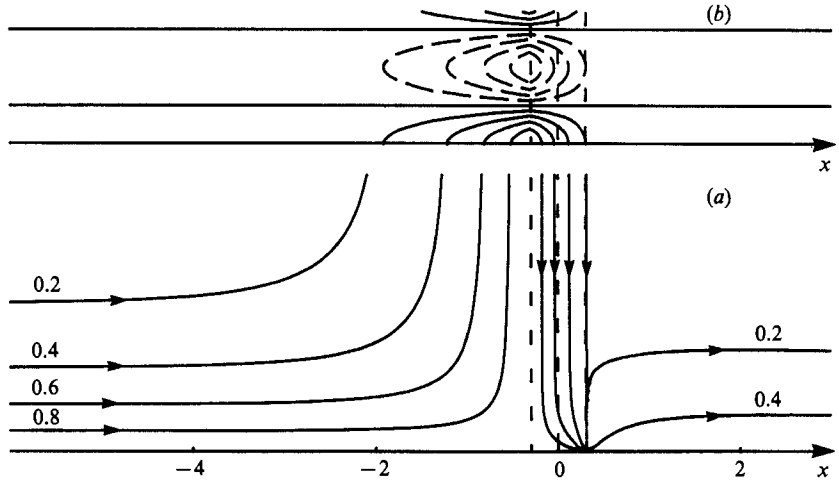

FIGURE 6. As for figure 4 but for a narrower ridge, of half-width $W = 0.3$. The outer wave field and the inner flow away from the ridge are barely altered. Above the ridge the flow is strongly confined by the steps, remaining parallel until close to the wall. The return flow above the ridge extends just outside the ridge and fluid with $p < 0.2$ joins the transmitted wave without passing through the singularity at $(W, 0)$.

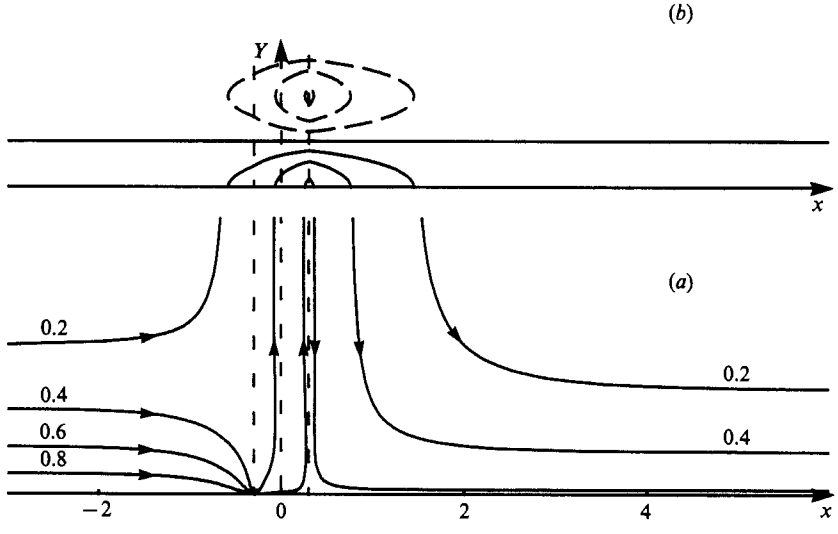

FIGURE 7. As for figure 5 but for a narrower valley, of half-width $W = 0.3$. The outward flow above the valley is now wider than the valley itself and about half the incident fluid turns to join the outward current without passing through the singularity at $(W, 0)$.

to a rapidly convergent sequence though it is not optimum. It is shown in II that more rapid convergence follows by dividing the profile into intervals within which $h'(x)$ is strictly one-signed and then choosing the positions of the steps to be at the Chebyshev points within each interval. Consider the smooth features of width W and depth at centre h_1, given by

$$h(x) = \begin{cases} 1 & |x| \geqslant W \\ h_1 + (1-h_1)\,(x/W)^{\epsilon} & |x| \leqslant W, \end{cases} \tag{5.9}$$

where ϵ controls the shape of the profile. Figure 8 gives the transmission amplitude

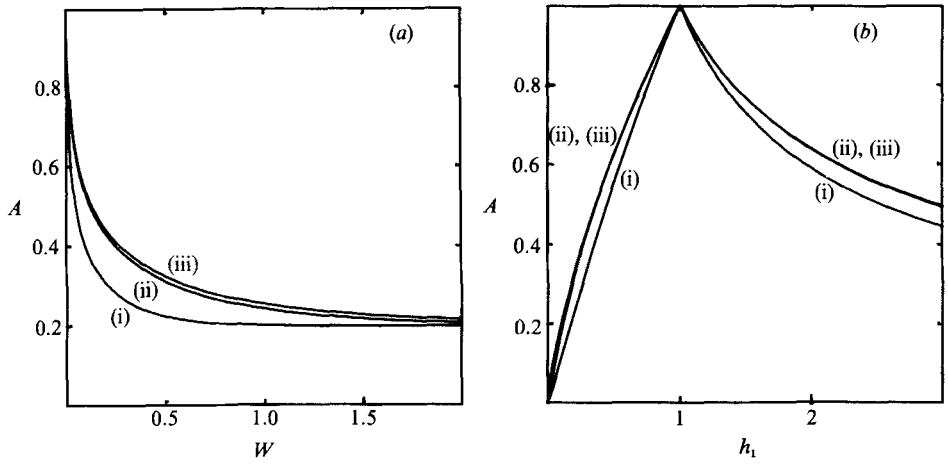

FIGURE 8. (*a*) The amplitude of the transmitted Kelvin wave for a high parabolic ridge with minimum depth $h_1 = 0.2$ as a function of the half-width W. (*b*) The amplitude for a ridge of half-width $W = 0.5$ as a function of the minimum depth h_1. The numbers n of steps used to approximate the ridge are (i) $n = 2$, (ii) 4, (iii) 10.

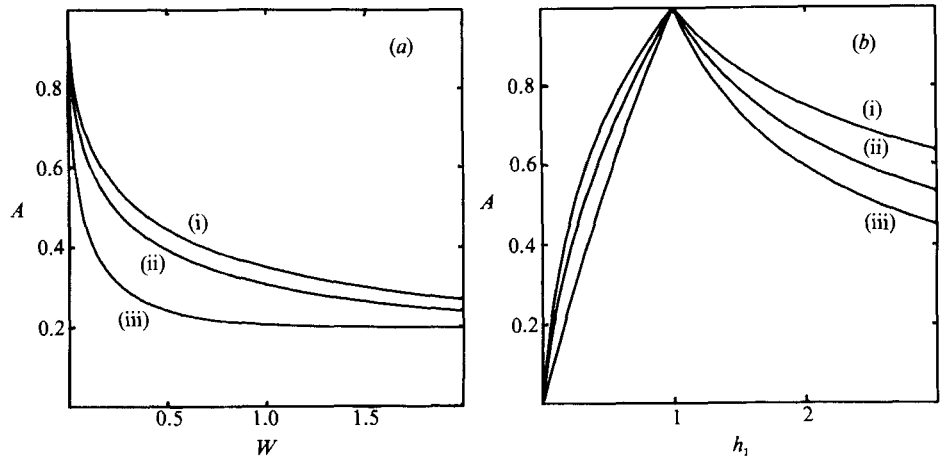

FIGURE 9. (*a*) The transmission amplitude A for ridges with minimum depth $h_1 = 0.2$ as a function of the half-width W. (*b*) The amplitude for a half-width $W = 0.5$ as a function of the minimum depth h_1. The volume of the topography changes from curve to curve: (i) $\epsilon = \frac{1}{10}$, a narrow concave-upwards profile; (ii) $\epsilon = 1$, a triangle ridge; (iii) $\epsilon = 10$, a broad concave-downwards profile.

as a function of W and of h_1 for a parabolic ridge ($\epsilon = 2$) for various numbers of steps. Except for the widest and highest of ridges, the results are graphically indistinguishable for $n > 4$. Accurately resolving the effects of rapid topographic oscillations requires approximately four steps per feature. Figure 9 gives the transmission amplitude as a function of W and of h_1 for various ϵ. For a given height the transmitted amplitude approaches its wide-ridge ($W \gg 1$) limit most rapidly for obstacles of largest volume. For a given height and width the blocking effect increases with volume.

Figure 10 gives the flow patterns above a parabolic ridge ($W = 1, h_1 = \frac{1}{2}, n = 12$). The ridge has been approximated by 11 constant-width strips and so by (3.4) the surface elevation in the inner region is identically equal to unity over the first five

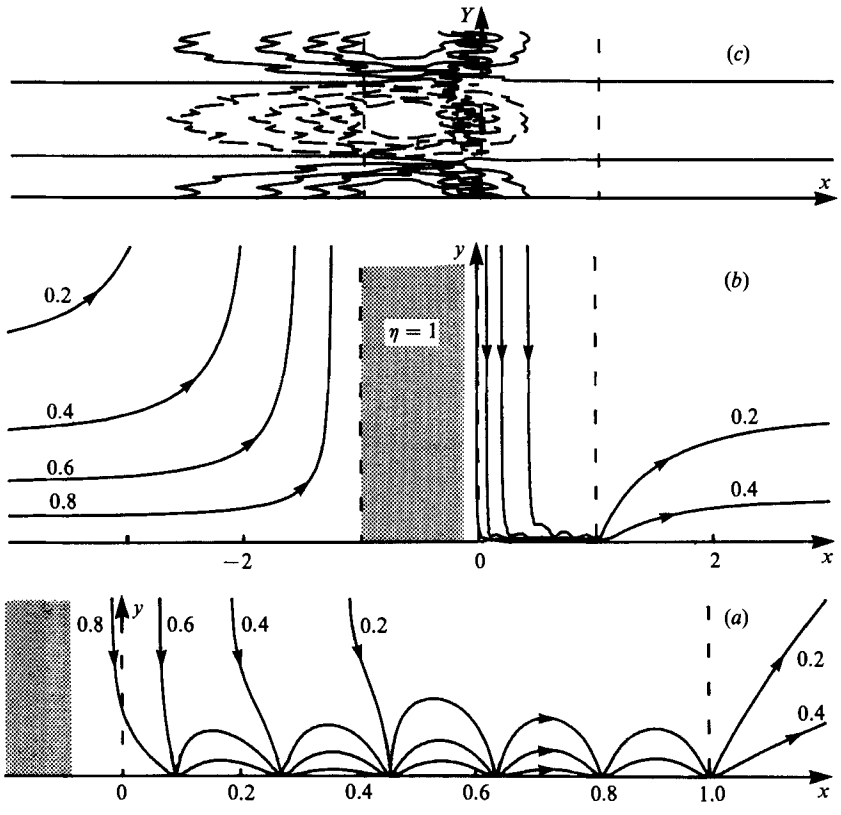

FIGURE 10. The flow patterns for a parabolic ridge of minimum depth $h_1 = \frac{1}{2}$ and half-width $W = 1$. (*a*) and (*b*) The streamlines of the inner solution with the stagnant region of surface elevation unity over the upslope of the ridge shown shaded. (*a*) is a detail of (*b*) magnified by a factor 5 to display the structure of the boundary-layer against the wall above the downslope of the ridge. (*c*) The corresponding outer flow showing the wave field concentrated above the upslope. The ridge has been approximated by twelve steps ($n = 12$).

(i.e. $-1 \leqslant x \leqslant -1/11$) and the flow is stagnant there. The flow returns above the downslope of the ridge, remaining parallel until close to the wall. Figure 10(*a*) shows the flow turning in a layer pinned against the wall at the six downward steps of the approximating stepped ridge and emerging through a source at (1, 0). The form of these wall–step singularities has been discussed in Johnson (1985). For continuous topography the stagnant region covers the entire upslope region, barring a layer of thickness $\omega^{\frac{1}{2}}$ or $\omega^{\frac{1}{3}}$ about $x = 0$ (depending on the shape of the ridge crest), and the entraining boundary layer above the downslope has thickness of order ω (Johnson 1989*a*, *b*). In the outer-y region the wave field is concentrated above the upslope. Although the wave field is generally dominated by longer wavelengths, much high-wavenumber structure is evident, particularly near the crest of the ridge. The pattern reproduces many of the features of the numerical simulation of Killworth (1989*a*) presented in his figure 3(*a*). The wide turning oncoming flow, the stagnant inner region above the upslope, the very narrow return flow after the crest and the reduced-width continuing flow of figure 10(*b*) are all visible as is the outgoing long wave, compressed in figure 10(*c*). The main differences are the termination of long wave in the numerical solution due to the inclusion of viscosity to prevent reflection

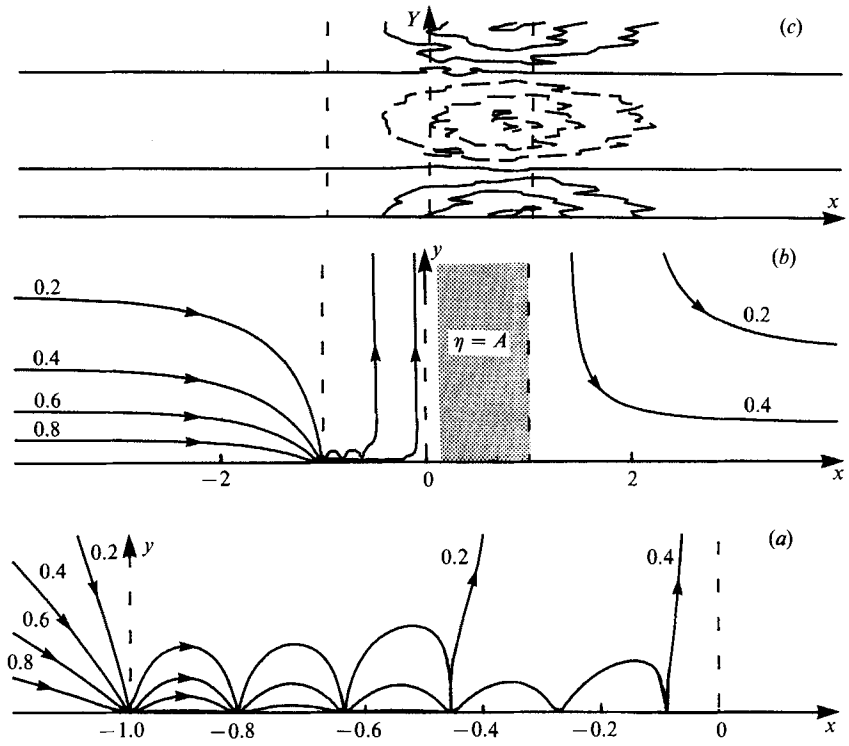

FIGURE 11. As for figure 10 but for a parabolic valley of maximum depth $h_1 = 2$. The stagnant shaded region of the inner solution has surface elevation A, the transmitted amplitude, joining smoothly to the transmitted wave in $x \geqslant 1$.

of energy at the rigid outer boundary of the computational domain and the presence of short waves above the downslope. It is shown in Johnson (1989*a*, 1990*a*) that these waves are absent in weakly dissipative flows and, in inviscid flows, although contributing to the outward energy flux carry no mass and so do not alter from the weakly dissipative determination the transmitted mass flux or consequently the amplitude of the transmitted Kelvin wave.

Figure 11 gives the flow above a parabolic valley ($W = 1, h_1 = 2, n = 12$). In the inner region the incident flux enters a sink at $(-W, 0)$ to be carried along by a detraining boundary layer pinned against the wall by the six downward steps. The region above the upslope between the six upward steps is stagnant with constant surface elevation $p = A$, the amplitude of the transmitted wave. As for rectangular topography, the amplitude of the outgoing waves in the outer-y region is given by the transmitted wave and so is weaker than the corresponding field for the ridge. Much high-wavenumber structure is again visible. The pattern propagates outwards at the speed of the lowest mode with periodic changes of form caused by the more slowly propagating higher modes. A more concise representation of the outer flow is thus given by considering the amplitudes and speeds of the component waves. Figure 12(*a*) gives the cross-ridge structure of the lowest three outwardly propagating modes (those with negative eigenvalues λ_j of smallest magnitude) for the ridge of figure 10 with, however, the number of steps increased to 30 to indicate how closely the stepped eigenfunctions approach continuous differentiability. Figure 12(*b*) gives the lowest three modes for the valley of figure 11. The decay of the modes away from the favourable slope above the valley is slower owing to the larger Rossby radius

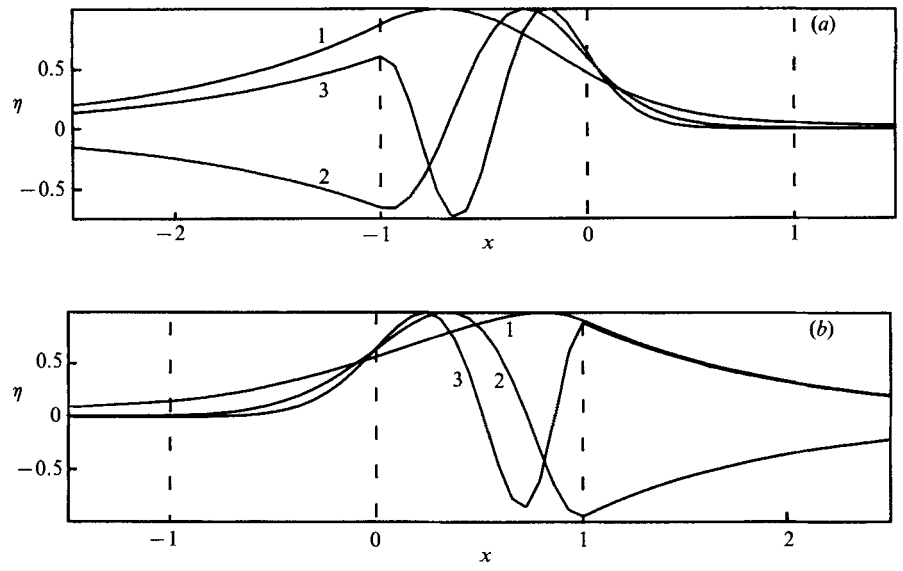

FIGURE 12. (*a*) The lowest three outwardly propagating modes (those three with negative eigenvalues of smallest magnitude) above the ridge of figure 10 ($n = 30$). (*b*) The lowest three outward modes for the valley of figure 11. In both cases the modes have no, one and two zero crossings and zeros of consecutive modes interlace.

Mode number	1	2	3	4	5	6
Ridge wave-number	4.773	27.92	70.38	114.2	138.0	349.6
Ridge wave amplitude	1.072	0.067	0.137	0.001	−0.052	0.189
Valley wave-number	3.315	27.73	66.31	104.8	202.6	659.6
Valley wave amplitude	0.622	−0.044	0.057	−0.023	0.030	0.077

TABLE 1. The wavenumbers and amplitudes for the six outwardly propagating waves of the outer-y field above the ridge of figure 10 and the six for the wave field above the valley of figure 11. The wave fields are dominated by the fundamental, which is 44% longer above the valley, but the slowly propagating very short waves carry some of the radiated energy.

there. The modes have no, one and two zero crossings and zeros of consecutive modes interlace. Longuet-Higgins (1968) discusses these waves for continuous monotonic depth changes and Killworth (1989*a*) considers some aspects for ridge-like topography. Further properties including completeness, orthogonality, zero crossings and interlacing are derived in II. Table 1 gives the amplitudes of the modes used to construct figures 10 and 11, showing the dominance of the lower modes and the insignificance of the higher modes. The highest wavenumber present is large and increases as the number of approximating steps increases. This does not affect the solution as its amplitude is small but points to the presence of finer structure in the limit of continuous topography. This structure is discussed in greater detail in II.

The patterns over more complicated features consisting of alternate ridges and valley are a combination of the two basic forms discussed above. Figure 13 gives the profile, stepped approximation and surface elevation along the wall for two valleys separated by a ridge. As in the previous examples, surface elevation decreases monotonically above downslopes and remains constant above upslopes.

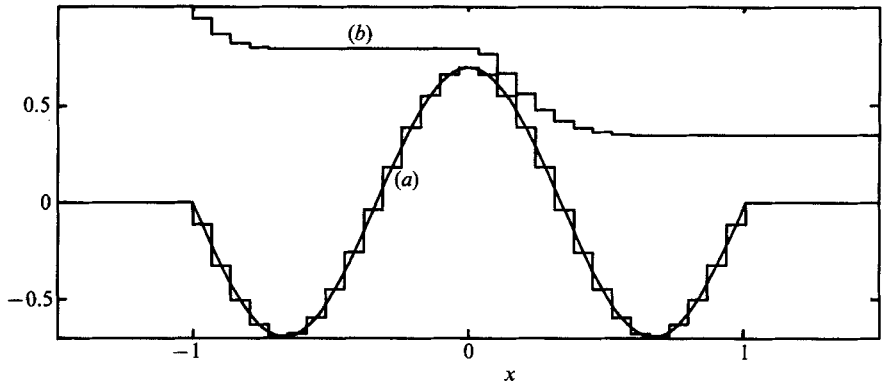

FIGURE 13. (*a*) The profile of the smooth obstacle with height $0.7\cos(\frac{3}{2}\pi x)$ and its stepped approximation with $n = 30$. (*b*) The corresponding surface elevation at the wall. The surface elevation decreases monotonically above downslopes, conserving mass flux, and remains constant above upslopes.

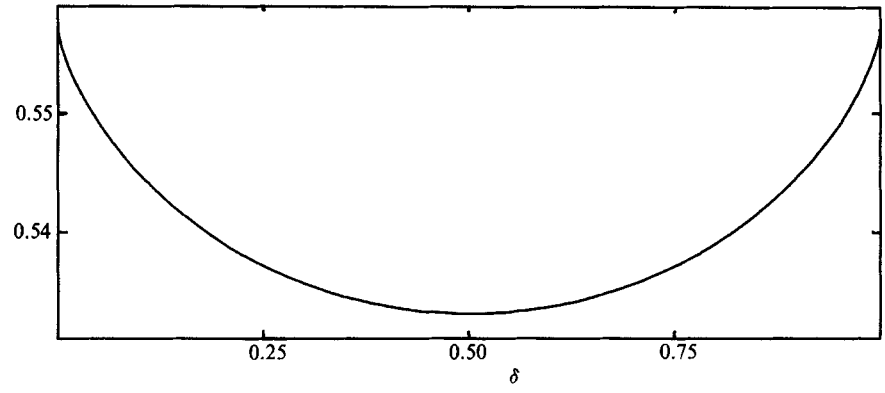

FIGURE 14. The transmitted amplitude A for topography consisting of two rectangular ridges each of minimum depth $h_1 = \frac{1}{4}$, the first of width δW and the second of width $(1-\delta)W$, separated by a distance W. The amplitude is given as a function of δ for $W = 0.1$. As δ increases from 0 the leading ridge thickens as the trailing ridge thins. The obstacle for any δ is the reflection about $x = 0$ of the obstacle for $1-\delta$.

For simplicity the examples to date have been chosen to be symmetric about $x = 0$. To assess the effect of asymmetry consider the obstacle with height

$$h(x) = \begin{cases} h_1 & \text{if} \quad -W < x < (\delta-1)W \quad \text{or} \quad \delta W < x < W \\ 1 & \text{otherwise,} \end{cases} \tag{5.10}$$

consisting of two ridges of width δW and $(1-\delta)W$ separated by a distance W. As δ increases from zero the obstacle changes continuously from a wide ridge following a thin ridge, through two equal ridges when $\delta = \frac{1}{2}$ to a thin ridge following a wide ridge at $\delta = 1$. Figure 14 gives the transmitted amplitude as a function of δ for $W = 0.1$ and $h_1 = 0.25$. The variation is less than 5%. For wider obstacles and for changes in single ridges from steep leading edge and shallow trailing side to the opposite, changes are even smaller. It appears that to a great extent the transmitted amplitude is determined by the size of the steps and not their relative ordering. Figure 14 is symmetric about $\delta = \frac{1}{2}$. This follows directly from the result in II that the

transmitted amplitude A' in the adjoint problem (obtained by reversing the direction of rotation) is related to the amplitude A by

$$H_0 A' = H_\infty A. \tag{5.11}$$

Thus if the far-field depths are equal the transmitted amplitude is unaffected by reflecting the topography about $x = 0$. If $H_0 \neq H_\infty$ then it is the transmitted volume flux that is unaffected by reflecting. In particular, this result allows either of (5.1) or (5.2) to be derived from the other.

6. Discussion

The problem of Kelvin wave scattering by ridge-like features abutting sidewalls has been simplified by restricting attention to the low-frequency limit and approximating more general features by stepped profiles. In this limit the problem divides naturally into three regions, the outer-x and outer-y regions containing the outwardly propagating long topographic waves and the quasi-steady inner region. The analyses of wall–step junctions in Johnson (1985), Gill *et al.* (1986) and Johnson & Davey (1990) show that surface height is continuous at upward steps and discontinuous at downward steps. Combining conservation of mass at wall–step junctions with the requirement that scattered energy propagates outwards gives a real linear system for the amplitude of the transmitted wave. The size of this system is proportional to the number of possible incoming topographic waves. Once this system is solved the form of the flow follows directly.

The inner region flows extend the steady solutions derived for single steps in Gill *et al.* (1986) to give streamlines for steady coastal currents turned outwards by non-monotonic features and predict the amount of current continuing. Moreover, the inner regions are geostrophic, satisfying the nonlinear equation for the conservation of potential vorticity everywhere except at the wall–step singularities and so should closely model observed flows set up by steady coastal currents.

It has been shown for the inner region that motion above downslopes is confined to a boundary layer against the sidewall and flow is stagnant above upslopes. This analysis extends directly to weakly dissipative flow over continuous topography, giving sidewall boundary layers of the form discussed in the context of low-frequency shelf-wave scattering in Johnson (1989*a*). Let dissipation be such that unforced vorticity decays over a time of order τ. If $f\tau \gg \omega^{-2}$ short waves are present in all regions; if $\omega^{-2} \ll f\tau \ll \omega^{-1}$ short-wave energy is destroyed at the wall but the geostrophic and long-wave regions are inviscid; if $\omega f\tau \sim 1$ long waves are affected by viscosity; and if $f\tau \sim 1$ the whole flow is affected. The extension of these results and the present analysis to Kelvin wave scattering over continuous ridges and the form of the short-wave field for completely inviscid flow are given in II.

For clarity the present results have been presented for topography meeting a straight sidewall perpendicularly. As shown in Johnson (1989*b*), the present method applies to arbitrary scattering regions provided the topography becomes rectilinear (i.e. isobaths become parallel) eventually with distance from the wall (figure 15). If all far-field isobaths (or step paths for stepped topography) reach the sidewall (figure 15*a*) then the conditions of the wall–step junctions and surface heights above the steps are unaltered and both the outer flow and transmission amplitude are unchanged from those for a straight perpendicular wall. If the inner, scattering region is more complex (figure 15*b*) then the connection of isobaths must be considered (Johnson 1989*b*). As a particular example consider a ridge of half-width

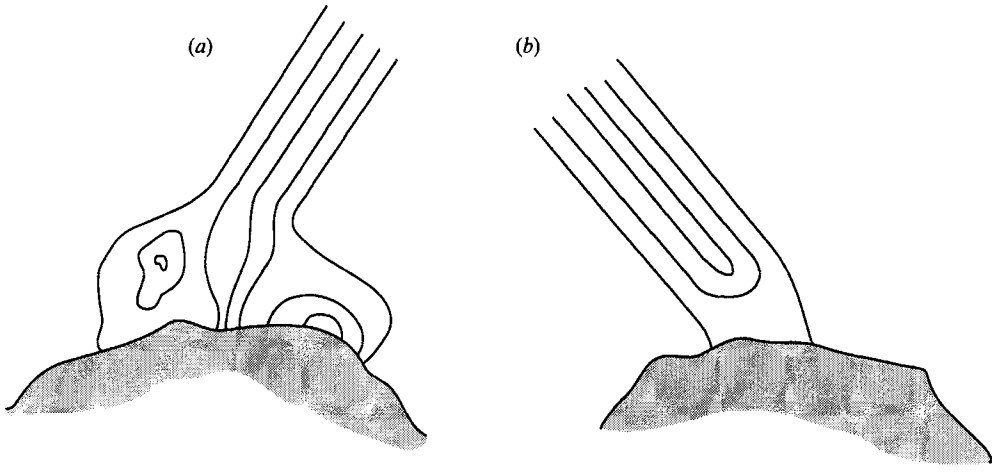

FIGURE 15. Isobaths that become parallel eventually with distance from the wall. (*a*) All incident isobaths reach the sidewall and so the outer flow and transmission amplitude are unchanged from those for rectilinear topography with a perpendicular wall. (*b*) Some incident isobaths fail to reach the wall and so connection formulae (Johnson 1989*b*) are needed to determine the outer flow.

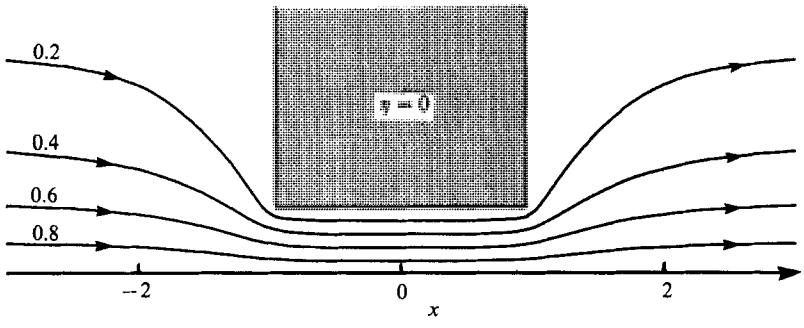

FIGURE 16. Streamlines for flow in the inner region past a rectangular ridge or valley of arbitrary height or depth ($h_1 \neq 1$) of half-width $W = 1$ terminating at a distance $D = \frac{1}{2}$ from the bounding wall $y = 0$. Flow in the far field and above the feature is stagnant and the incident Kelvin wave passes through the gap with unaltered amplitude and phase.

W terminating abruptly at a distance D from the wall (figure 16). Then by geostrophy η is constant along the isobath in the inner region, and so the outer limit of the inner solution has equal values of η on the isobaths. In the outer region the values of η on the isobaths are in the ratio 1 to $\gamma \neq 1$ by (5.4). Compatability thus requires that η vanishes on the isobath and hence the outer region is stagnant. A ridge of arbitrary height not reaching the wall behaves as a solid barrier. Along the wall in the inner region η is constant and the transmitted wave has unit amplitude. Figure 16 includes streamlines of the inner flow which satisfy

$$\nabla^2\eta - \eta = 0 \quad (y \geqslant 0) \quad \text{outside ridge}, \tag{6.1}$$

$$\eta \equiv 0 \quad \text{above ridge}, \tag{6.2}$$

$$\eta = 1 \quad (y = 0). \tag{6.3}$$

This topography gives an example of a ridge where the upper bound of Killworth (1989*a*) is exceeded. For a given far-field profile the transmitted amplitude is

increased if a cross-ridge gully, not necessarily of the full fluid depth as above, is present. Similarly transmission across a valley is increased if a cross-valley bridge is present. The increase in transmission occurs independently of the position of the gully or bridge and not only when they occur against the bounding wall as in this example. The dynamics of the outer and geostrophic regions are coupled and bounds derived considering the outer region alone do not apply to features of the form of figure 15(*b*). The inner solution conserves potential vorticity and so represents steady flow at arbitrary amplitude, pointing to strong flows through narrow gaps in ridges and over thin bridges across valleys.

The analysis has been presented for a homogeneous fluid with a free surface and so models the lower layer of a two-layer fluid with an inert, infinitely deep upper layer. As the equations for multi-layered flow separate above stepped topography the present results extend simply and directly to give explicitly the wave fields and transmission amplitudes for scattering of internal Kelvin waves incident on a ridge. Killworth (1989*b*) presents numerical computations and bounds for two-layer flows with a rigid lid but notes the difficulty of extending the bounds to flows with more degrees of freedom.

Appendix. Numerical methods

The computations for a general solution break down into a series of standard steps. The first is to obtain the eigenvalues of (4.11). This follows most straightforwardly by rewriting (4.11) as

$$\boldsymbol{D}\boldsymbol{f} = l^{-1}\boldsymbol{A}\boldsymbol{f}, \tag{A 1}$$

and using a standard QR decomposition routine, preserving the reality of λ_j^{-1} since $\boldsymbol{D}$ is diagonal and $\boldsymbol{A}$ tridiagonal positive definite. Routine F02FHF of the NAG library makes explicit use of the banded form of $\boldsymbol{A}$ and $\boldsymbol{D}$ and proved very efficient in practice. The second step is to obtain the eigenvectors corresponding to outgoing waves (i.e. $\lambda_j^{-1} < 0$). These were obtained individually using NAG routine F02SDF. Thirdly the matrix $\boldsymbol{E}$ is formed and postmultiplied by $\boldsymbol{DB}$. The most straightforward solution of (4.17) follows by setting $b_0 = 1$, corresponding to an incident wave of unit amplitude, and solving the resulting $m \times m$ system for $b_1, \ldots, b_m$, using a standard solver such as the NAG routine F04ATF. If only the transmitted amplitude b_m is required the computation is complete. The free-surface heights η_j can be obtained from (3.8) and the amplitudes of the outwardly propagating long waves follow sequentially by obtaining the corresponding eigenvector using F02SDF and forming the ratio of inner products (4.19).

The flow pattern in the inner-y region follows by writing (3.13) as

$$\eta = a_j \exp(-h_j^{-\frac{1}{2}} y) + F(\boldsymbol{\eta}; x) \operatorname{erf} y + \frac{2}{\pi}\int_0^\infty Q(x, l) \sin ly \, \mathrm{d}l, \tag{A 2}$$

where $\operatorname{erf} y$ is the error function and $Q(x, l) = P(x, l) - F(\boldsymbol{\eta}; x) \exp(-\frac{1}{4}l^2)/l$ is bounded for all l, vanishing exponentially as $l \to \infty$ for $x \neq x_j (j = 1, \ldots, n)$. Thus (A 2) is in a form for rapid inversion by fast Fourier transforms.

REFERENCES

GILL, A. E., DAVEY, M. K., JOHNSON, E. R. & LINDEN, P. F. 1986 Rossby adjustment over a step. *J. Mar. Res.* **44**, 713–738.

GOLUB, G. H. & VAN LOAN, C. F. 1983 *Matrix Computations*, Chapter 7. North Oxford Academic.

HUTHNANCE, J. M. 1975 On trapped waves over a continental shelf. *J. Fluid Mech.* **69**, 689–704.

JOHNSON, E. R. 1985 Topographic waves and the evolution of coastal currents. *J. Fluid Mech.* **160**, 499–509.

JOHNSON, E. R. 1989*a* Boundary currents, free currents and dissipation regions in the low-frequency scattering of shelf waves. *J. Phys. Oceanogr.* **19**, 1293–1302.

JOHNSON, E. R. 1989*b* Connection formulae and classification of scattering regions for low-frequency shelf waves. *J. Phys. Oceanogr.* **19**, 1303–1312.

JOHNSON, E. R. 1989*c* The scattering of shelf waves by islands. *J. Phys. Oceanogr.* **19**, 1313–1318.

JOHNSON, E. R. 1989*d* Topographic waves in open domains. Part 1. Boundary conditions and frequency estimates. *J. Fluid Mech* **200**, 69–76.

JOHNSON, E. R. 1990*a* Energy conservation in low-frequency scattering of shelf-waves. *J. Phys. Oceanogr.* (submitted).

JOHNSON, E. R. 1990*b* Kelvin wave scattering and long waves over smooth topography. *J. Fluid Mech.* (submitted) (referred to as II).

JOHNSON, E. R. & DAVEY, M. K. 1990 Free surface adjustment and topographic waves in coastal currents. *J. Fluid Mech.* (in press).

KILLWORTH, P. D. 1989*a* How much of a baroclinic coastal Kelvin wave gets over a ridge? *J. Phys. Oceanogr.* **19**, 321–341.

KILLWORTH, P. D. 1989*b* On the transmission of a two-layer coastal Kelvin wave over a ridge. *J. Phys. Oceanogr.* **19**, 1131–1148.

LONGUET-HIGGINS, M. S. 1968 Double Kelvin waves with continuous depth profiles. *J. Fluid Mech.* **34**, 49–80.

MILES, J. W. 1972 Kelvin waves on oceanic boundaries. *J. Fluid Mech.* **55**, 113–127.

MILES, J. W. 1973 Kelvin-wave diffraction by changes in depth. *J. Fluid Mech.* **57**, 401–413.

TAYLOR, G. I. 1921 Tidal oscillations in gulfs and rectangular basins. *Proc. Lond. Math. Soc.* **20**, 148–181.

THOMSON, W. 1879 On gravitational oscillations of rotating water. *Proc. R. Soc. Edinburgh* **10**, 92–100.